International Journal of Environment Volume : 06 | Issue : 01 | Jan.-Mar. | 2017
ISSN: 2077-4508 Pages: 01-15

$ZnAl_2O_4$ nanoparticle surface: A promising adsorbent for the removal of toxic Chicago Sky Blue dye from water

[1]Saleh D. Mekkey and [2]A. A. Swelam

[1,2]Department of Chemistry, Faculty of Science, Al-Azhar University, Cairo, Egypt

Received: 25 November 2016 / Accepted: 30 December 2016 / Publication date: 07 January 2017

ABSTRACT

In this research, $ZnAl_2O_4$ nanocrystals were successfully synthesized by modifying Pechini method and characterized by FTIR, SEM, XRD methods and N_2 adsorption/desorption isotherms (BET). The composition of the mixed metal oxide was obtained by EDX analysis and its adsorption activity was evaluated in the removal of the textile dye, Chicago Sky Blue (CSB) dye from aqueous solution as an anionic dye in a batch system. Several conditions such as initial dye concentration, adsorbent dosage, contact time, solution pH, and temperature were investigated. The adsorption kinetics were studied using classic three equations of pseudo-first-order, -second-order and intraparticle diffusion models. The dynamical data fit well with the pseudo-second-order kinetic model. The negative value of the changes in enthalpy ($-\Delta H°$), the negative value of Gibbs free energy ($-\Delta G°$), showed that the adsorption is exothermic and spontaneous for all the studied temperatures. The equilibrium adsorption data were analysed using four adsorption models: Langmuir, Freundlich, Temkin and Dubinin–Radushkevich (D-R). The results showed that Langmuir isotherm fits the experimental results very well with high correlation coefficients. The maximum adsorption removal of CSB dye was 99.15% of the experimental conditions. This result is of practical interest, with respect to the selection of sorbent, to optimize aquatic environmental remediation technologies.

Key words: CSB dye; Removal; Kinetics; Thermodynamic

INTRODUCTION

The release of various ions of harmful dyes into the environment has attracted great attention worldwide in recent years because of their toxicity and extensive use. Numerous industries like the plastics, paper, textile and cosmetics utilize dyes to colour their goods. Dyes usually have a synthetic origin and complex chemical structure that makes them persistence to light, oxidation and biodegradable process (Carmen *et al*., 2017; Petrick *et al*., 2017; Mayur *et al*., 2017). Indeed, many dyes were developed for their chemical invariability and do not suffer from biochemical degradation easily. Moreover, many dyes are considered to be toxic to some organisms and may cause direct annihilation of aquatic communities. In addition to their unwanted colors, some of the dyes may break down to yield carcinogens and toxic compounds. Nowadays, more than one hundred thousand kinds of commercial dyes are used in the production of over 9 million tons annually (Mayur *et al*., 2017). Therefore, improving a sustainable method for the removal of color from effluents containing various kinds of synthetic dyes has long been a challenge for scientists. In particular, many efforts have been made to develop different kinds of materials to remove dyes from drinking water.

Different methods have been used for dye removal from wastewaters such as biological degradation (Fan *et al*., 2017), photocatalytic degradation (Lin *et al*., 2017), coagulation (Xin *et al*., 2017a), membrane filtration (Bouazizi *et al*., 2017), reverse osmosis (Yue *et al*., 2017), ozone treatment (Mena *et al*., 2017), adsorption (Muhammad *et al*., 2017), or the synergy treatment using different methods. Among these methods, the adsorption process is one of the most effective techniques that has been successfully employed for color removal because it is considered to be less expensive, more efficient and less likely to generate secondary waste (Zhenzhen *et al*., 2017).

Most conventional adsorption systems use activated carbon despite its high production costs and regeneration difficulty. As one alternate effective process, adsorption technology has been regarded as

Corresponding Author: Saleh D. Mekky, Department of Chemistry, Faculty of Science, Al-Azhar University, Cairo, Egypt
E-mail: salehsdmm@yahoo.com

one of the most promising and widely used methods due to its effectiveness, efficiency, economy and no secondary pollution. A number of materials, including metal oxides and hydroxides (Sneha *et al*., 20170; Wei *et al*., 2017), agricultural wastes (Thines *et al*., 2017), clays (Dordio *et al*., 2017), Chitosan (Agnès *et al*., 2017), silica (Zhijie *et al*., 2017), kaolinite (Xin *et al*., 2017b), sepiolite (Sílvia *et al*., 2016), graphene oxide (Yunchuan *et al*., 2017), active carbon (Somayeh *et al*., 2017), montmorillonite (Boran *et al*., 2017), zeolites (Lu *et al*., 2017) and some natural biosorbents (Ying-Lung *et al*., 2017). However, these materials generally have low adsorption capacities, and hence, a large adsorbent dosage is required to achieve a low dye concentration in the treated effluents.

Many of the authors reported that calcination markedly improved the solute uptake by layered double hydroxides LDHs (Wei *et al*., 2017; Chunsheng *et al*. 2017). The improvement was extensively explained by the dehydration of the calcined LDHs in water, "memory effect", and the increased specific surface area after calcination. However, the mechanisms of the adsorption process onto calcined LDHs, are still not clear.

Chicago sky blue, also known as Niagara sky blue, is a vital dye that can successfully be used as an intravascular energy absorbing target for the light from a helium-neon laser. The result of this light/dye interaction is endothelium damage which can be controlled by adjusting the duration of the laser exposure and the amount of dye injected intravenously. The endothelial damage probably is the result of the heat generated by the dye absorption of energy at the interface between plasma and endothelium. The most minimal damage resulted in selective loss of the dilation normally produced by acetylcholine and bradykinin, two endothelium dependent dilators. The dilation produced by sodium nitroprusside, a dilator acting directly on vascular smooth muscle, was preserved. More severe injury, i.e. more prolonged exposure to light and/or more dye, resulted in local platelet aggregation at the site of laser impact (Nishimura *et al*., 1989).

Chicago Sky Blue 6B (CSB) with IUPAC names of sodium 4-[(4-dimethylamino) phenyldiazenyl] benzene sulfonate (Scheme 1) is a typical water-soluble anionic.

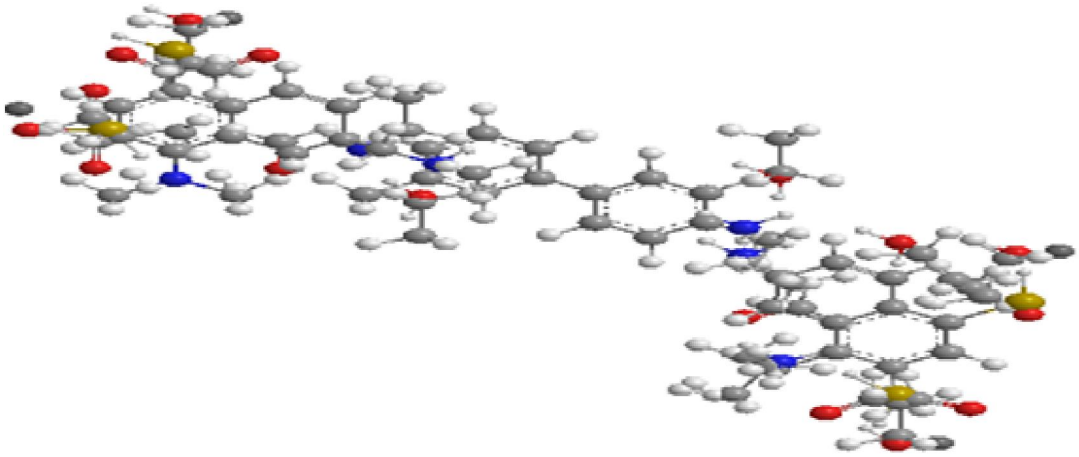

Scheme 1: 3D of Chicago Sky Blue B6 Dye

In the present work, zinc, aluminium-mixed oxide was synthesised via a modified Pechini method and used as an adsorbent of Chicago Sky Blue dye (CSB) after calcination at 800^0C. The sample was characterised by powder XRD, FTIR, SEM and EDX. The effects of various parameters such as adsorbent dose, solution pH, contact time, dye concentration and temperature on the removal of Chicago Sky Blue dye by these precursors were studied in detail. The adsorption kinetic data were tested by pseudo-first-order, pseudo-second-order and intraparticle diffusion kinetic models. The equilibrium data were analysed using the Langmuir, Freundlich, Temkin and Dubinin–Radushkevich (D-R) isotherm models. Thermodynamic parameters were also evaluated at three different temperatures.

Experimental details:

Chemicals and reagents:

All of the reagents were of analytical grade with the mass fraction purity of 0.99 and used as received without further purification. $AlCl_3$, zinc acetate, citric acid, Ethylene glycol, HCl and NaOH were purchased from British Drug House, Poole, England.. The anionic sulfonated azobenzene dye used in these experiments is Chicago Sky Blue 6B (CSB). CSB (Molecular weight 992.82, purity >99%) were purchased from Aldrich Chemical Co., USA and handled using proper safety procedures. It was used without further purification and chemical structures are shown in Scheme 1. Chicago Sky Blue 6B stock solutions (100 mg /l) was prepared by dissolving the required amount in double distilled water and the working solution was prepared daily with the required dilution..

Powder preparation:

Aluminium chloride [$AlCl_3$] and zinc acetate [$Zn(CH_3COO)_2.2H_2O$] were dissolved in distilled water and citric acid (CA) was then added (molar ratio CA: total cations = 1). The mixture was magnetically stirred until a clear yellowish solution was obtained. Ethylene glycol (EG, M.Wt = 62.07) was added to this solution in the molar ratio EG: CA = 2. The solution was continuously stirred at around 80 °C in order to facilitate the evaporation of the excess water and accelerate the polyesterification reaction. During the polyesterification process no turbidity or precipitation was observed. The procedure was stopped when a viscous gel was obtained. The gel was then heated at 150 °C in an oven for 24 h. The xerogel was ground and calcined at 800 °C for 6 h to obtain the $ZnAl_2O_4$ powder.

Characterization of $ZnAl_2O_4$ nanoparticles:

The prepared product was characterized using X-ray diffraction (XRD), scanning electron microscopy (SEM), energy dispersive X-ray analysis (EDAX), surface area determination using BET analysis and FTIR analysis. Scanning electron microscope (SEM) analysis was performed with a Quanta 250 FEG (Field Emission Gun) attached with EDX Unit (Energy Dispersive X-ray Analyses), with accelerating voltage 30 K.V., magnification14x up to 1000000 and resolutions for Gun.1n). Infrared spectrum (IR) was obtained using a JASCO 6100, made in Japan infrared spectrometer. X-ray diffraction (XRD) pattern was measured at room temperature by using a Philips diffractometer (type PW-3710). The patterns were run with Ni-filtered copper radiation (θ = 1.5404 Å) at 30 kV and10 mA with a scanning speed of 2θ = 2.5◦/min. The mean particle size was calculated using the Debye–Scherrer Eq. [$(K\lambda)/(\beta\cos\Theta)$], in which K is a constant equal 0.9, λ is the wavelength of the Cu Kα radiation, β is the half peak width of the diffraction peak in radiant.

Adsorption experiments:

Batch experiment for Chicago Sky Blue (CSB was carried out in the dark to avoid photolysis at the natural pH. Natural pH was measured in aqueous media without any addition of external ions. A stock solution of 100 ppm was prepared and kept in the dark. This was used for adsorption studies after appropriate dilution. The amount of adsorbent was kept constant at 0.2 g/100 ml unless otherwise mentioned. The solution was continuously stirred at 400–500 rpm to maintain homogeneity throughout the solution. Sodium hydroxide and hydrochloric acid were adopted to adjust the solvent pH value before adsorption experiments. The effect of contact time (0–300 min), initial pH value (2-12), initial concentration of (CSB) (30–100 mg/L) on the adsorption performance were investigated. 100 ml (CSB) solution with a certain concentration was added in the 150 ml conical flask.

The samples were taken out at suitable intervals for the measurement of concentration of dye in liquid phase. The aliquots were centrifuged to remove the adsorbent particles and the absorbance was measured using UV–vis spectrophotometer (UV 1700, Shimadzu, Japan) at the characteristic wavelength (λ) of the dye (CR-497 nm, OG-480 nm, IC-610 nm, MB-600 nm). The calibration based on Beer Lambert's law was used to convert absorbance to concentration. The absorbance varied

proportionally with dye concentration as absorbance = A × concentration. The values of A were varied for CSB, and this calibration is valid up to dye concentration of 30 mg/l. For higher concentrations, dilution was carried out and accordingly the concentration was obtained by multiplying by the dilution factor.

The adsorption capacity and removal ratio of adsorbent can be calculated according to the Eqs. (1) and (2), respectively:

$$q_t = \frac{(C_0 - C_e)\,v}{m} \quad (1)$$

$$R = \frac{Co - Ce}{Co} \quad (2)$$

where q_t is the adsorption capacity at the time t, mg/g; C_0 and C_e are the initial and equilibrium concentration of (CSB), mg/L; R is the removal ratio, %; V is the volume of solution, L and m is the dose of adsorbent sample, g.

Results and Discussion

Characterization of the adsorbent:

The mixed oxide $ZnAl_2O_4$ nanoparticle was further characterized by FTIR analysis. Fig. 1. Fig. 1 shows the FT-IR spectra of the calcined product. From this Figure, the bands at 3500 cm^{-1} and 1384 cm^{-1} are not present in the calcined sample, which are attributed to the removal of water molecules and the decomposition of the NO_3^- groups in the mixed oxide $ZnAl_2O_4$ interlayer. In the calcined sample, the bands at 497, 564 and 677 cm^{-1} are related to Al─O bonds in the $ZnAl_2O_4$ phase (Xiaoyun *et al*., 2012). The bands at 683, 564 cm^{-1} are assigned to the stretching modes of AlO_6 octahedral units, and the band observed at 495 cm^{-1} is due to the bending mode of AlO_6 octahedral units (Mei-Yu *et al*., 2013).

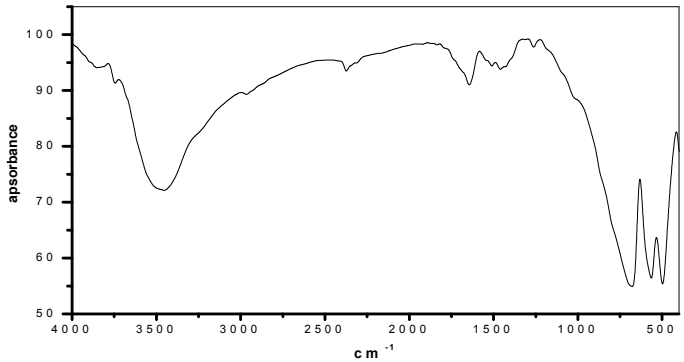

Fig.1. FTIR plot of the adsorbent

Morphology of the $ZnAl_2O_4$ nanostructures was investigated with SEM as shown in Fig. 2. The prepared nanosized particles are well dispersed and similarly spherical. The corresponding particle size distribution (inset in Fig. 2) indicates the average diameter of $ZnAl_2O_4$ is about 24.12 nm. The EDAX is shown in Fig. 3. The results show that the mixture is uniform as the image shown and the atomic % of aluminium is around 2 times of that of zinc. This confirms the formation of $ZnAl_2O_4$.

The XRD patterns for $ZnAl_2O_4$ are shown in Fig. 4. All the diffraction peaks can be perfectly indexed to face-centred cubic spinel-structured $ZnAl_2O_4$. The diffraction peaks of the produced powders and that of standard were the same. This indicates that there is a complete formation of the spinel phase in all the samples synthesized in the experimental conditions employed in this work. No impurities were detected in the samples synthesized. The average crystallite size was estimated by applying the Scherrer formula on the highest intensity peak for each sample. An average size of around 10–20 nm was obtained for the sample. Therefore, XRD results provide further support for the formation of a $ZnAl_2O_4$ spinel during calcination, which is in good agreement with FT-IR spectra.

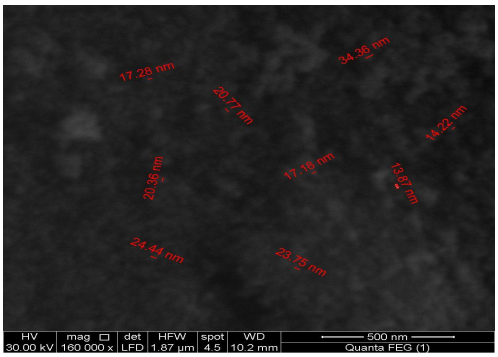

Fig. 2: SEM of the adsorbent

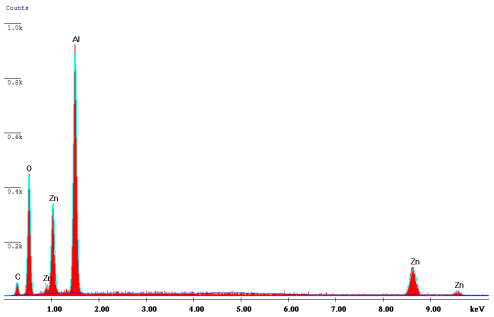

Fig. 3: EDX of the adsorbent

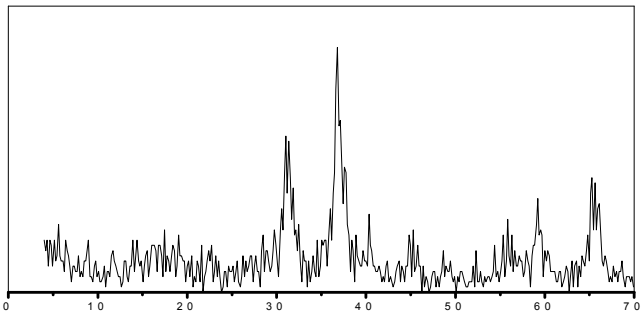

Fig. 4: XRD of the adsorbent

Nitrogen adsorption–desorption isotherms for the $ZnAl_2O_4$ sample prepared is displayed in Fig. 5. According to IUPAC classification, the isotherms for samples are of type IV, representing predominantly mesoporous structure characteristics. The mesoporous structure was confirmed by the analysis of pore size distribution (Table 1), which shows the spectra of the pore diameter with the defined maxima in the mesoporous region of the sample. The pore size distribution curve displays a wide unimodal distribution with an average pore size ranged from 13.87 to 34 .36 nm for the sample. In addition, the total pore volume was 0.0635 cc/g. The value of the BET surface area is also determined. The sample obtained by the co-precipitation method had a relatively small area at approx. 79.24 m^2 g^{-1}. These features are of great importance for the adsorption purposes because it allows for a greater accessibility of reactant molecules to the oxide material. For comparison purposes, the value of surface area found in the literature for the $ZnAl_2O_4$ oxide prepared from co-precipitation, was 86 (Farhadi *et al*., 2010), and 90 m^2 g^{-1} (Edson *et al*., 2012), respectively. It can be said that combustion synthesis led to the formation of nanoparticle zinc aluminium oxides.

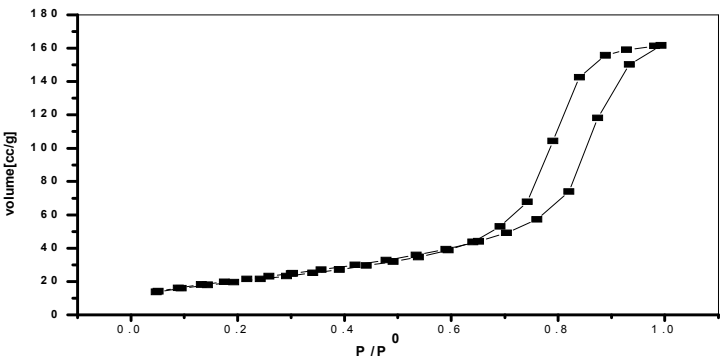

Fig. 5: BET of the adsorbent

Effect of pH on Chicago Sky Blue adsorption:

The initial pH of the solution affects the structural stability of the dye molecules and the surface charge on the adsorbent. These two conditions in turn influence the adsorptive removal of the dye from its aqueous solution. Fig. 6 shows the effect of pH on the adsorption of Chicago Sky Blue onto the adsorbent. It can be observed that the maximum dye removal efficiency of the adsorbent was 99.57% occurs around pH 7.8 (± 0.2). The original pH of the Chicago Sky Blue solution (70 mg/L) is about 6.7.

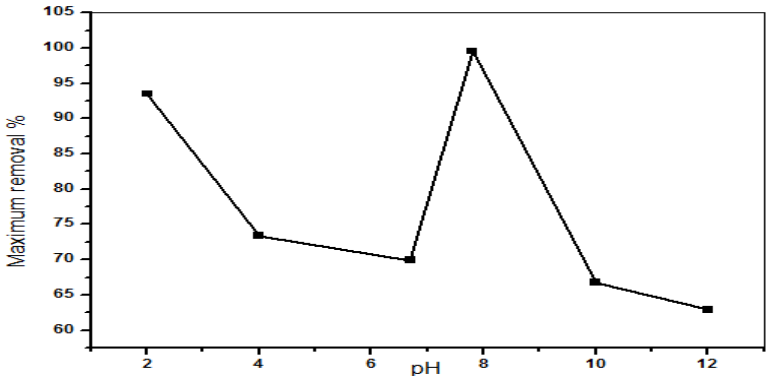

Fig. 6: Effect of pH values on the % removal of CSB dye

It was seen that the dye solution changes its colour from dark blue to red when pH was adjusted in the highly acidic range and becomes pale blue in highly basic range i.e., pH 10 and above. Therefore, the pH value for Chicago Sky Blue adsorption was kept in the 7.8 (± 0.2). On the other hand, the observed change in CSB color and absorbance intensity with the change of acidity or alkalinity of CSB dye solution (Fig. 7) is indicative of a structural change in the molecular form of the dye (Mane *et al*., 2013).

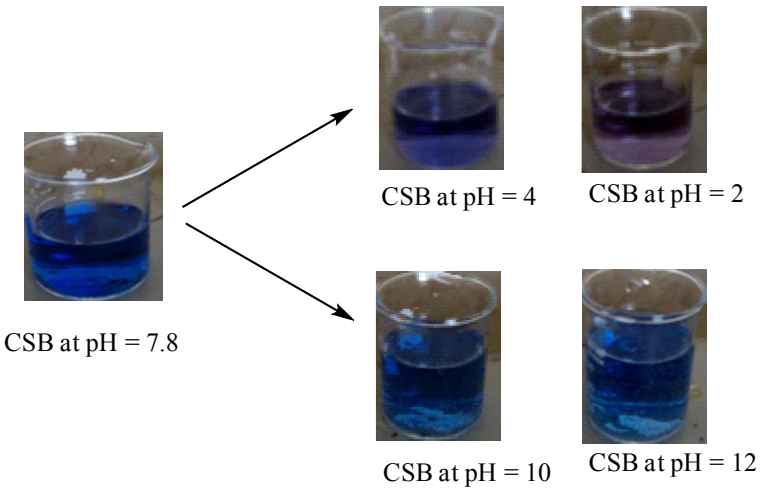

Fig. 7: Change in the Chicago Sky Blue color at different pH values

In the aqueous solution, the acid dye is first dissolved and the sulfonate groups of the acid dye ($D{-}SO_3Na$) are dissociated and converted to anionic dye ions at natural solution around pH 6 (Mane *et al*., 2013) according to Eq.3.

$$D - SO_3Na \xrightarrow{H_2O} D - SO_3^- + Na \quad (3)$$

As the pH of the solution increases, the number of positively charged sites decreases, thereby retarding the adsorption of the anionic dye molecules. Furthermore, in the alkaline conditions, the presence of excess –OH ions destabilize the anionic dye molecules and compete with the latter for positively charged binding sites. Above pH 7.8 (± 0.2) for the adsorbent, the surfaces of the adsorbent become negatively charged, resulting in an electrostatic repulsion between the dye

molecules and sorbent. This leads to a lower uptake of the Chicago Sky Blue dye molecules. However the fact that significant amount of adsorption is still observed suggests that electrostatic attraction is not the sole mechanism responsible for Chicago Sky Blue removal.

The Chicago Sky Blue molecule is bipolar (H_3N^+-R-SO_3^-) under low pH conditions. Pigorsch *et al*. 2013 reported that Congo red (CR) exists in two protonated (tautomeric species) form. In the first form (ammonium form), protons are attached to the ammonium nitrogen while in the second form (azonium form) the protons are attached to the α-azo group. In the azonium form CR molecule becomes cationic. The Fe–OH sites in the mixed oxides are negatively charged above pH 7.0 (pH_{zpc} Fe_2O_3 ~ 6.5) and therefore the cationic form of CR is also adsorbed by both the adsorbents at pH greater than7.0. This support higher removal efficiency observed at high pH in this study. Similar observations of colour change with a variation of pH were reported by several authors, Erol *et al*., 2017: Agnès *et al*., 2017: Hemant *et al*., 2017.

Effect of initial dye concentration and contact time:

Removal of Chicago Sky Blue for different initial concentrations as a function of contact time was studied and the result is shown in Fig. 8. Colour removal of the Chicago Sky Blue solution onto the adsorbent by adsorption was rapid initially and then slowed down gradually until it attained equilibrium on the surface of the $ZnAl_2O_4$ nanoparticles and solution phase. It was apparent from Fig. 8 that the amount uptake of dye (qt,mg/g) increased with the increase in the initial concentration of the dye. In principle, the initial dye concentration provided the necessary driving force to overcome the resistance to the mass transfer of the dye between the aqueous phase and the $ZnAl_2O_4$ nanoparticles. The increase in the initial dye concentration also enhanced the interaction between the dye and the $ZnAl_2O_4$ nanoparticles. Therefore, an increase in the initial concentration of CSB enhanced the adsorption uptake of the dye (Yunchuan *et al*., 2017). This could be explained due to an increase in the driving force of the concentration gradient, as an increase in the initial CSB concentration. This result revealed that the adsorption of CSB is fast and the equilibrium was achieved by 300 min of contact time. Considering these results, a contact time of 300 min was chosen for further experiments.

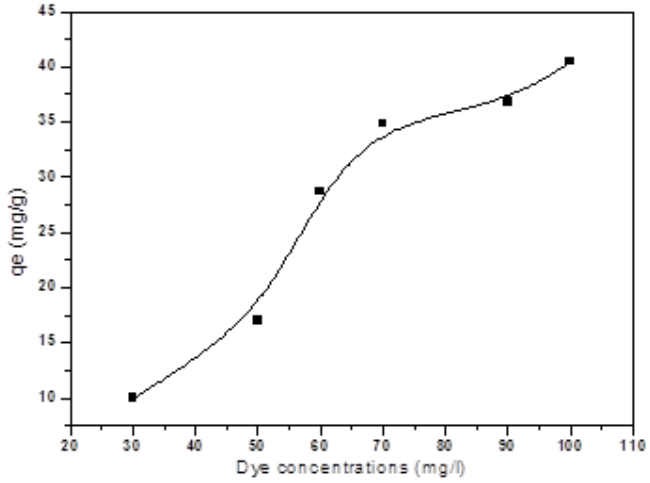

Fig. 8: Effect of the initial concentrations of CSB on the dye uptake (mg/g)

Effect of adsorbent dosage:

The effect of adsorbent dosage was studied on the Chicago Sky Blue removal from aqueous solutions by varying dosage of the adsorbent from 0.1 to 0.4 g/100 ml solution at a fixed initial concentration of 70 mg L^{-1}. The corresponding result is shown in Fig. 9. It showed that an increase in adsorbent dosage could increase the colour removal efficiency (%) from the solution. With increasing adsorbent dosages, more surface area was available for adsorption due to the increase in active sites

on the surface of the adsorbent and thus making easier penetration of adsorbate to adsorption sites (Ebrahim *et al*., 2017; Khadijeh *et al*., 2017).

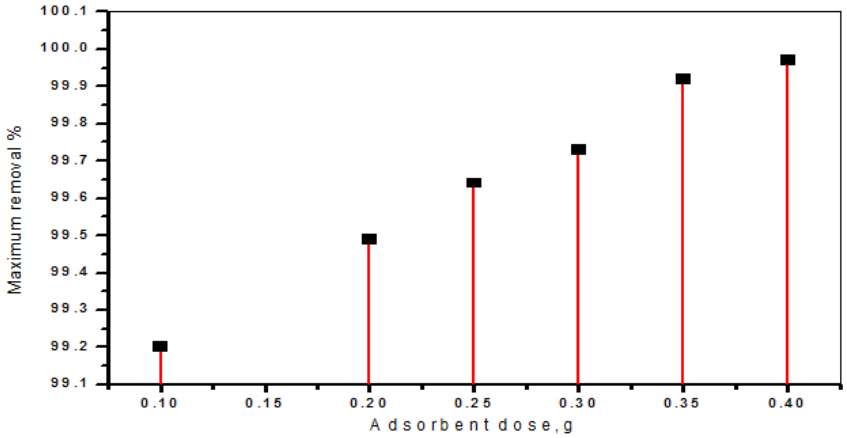

Fig. 9: Effect of adsorbant dose on the maximum removal percentage

The distribution ratio (D):

Distribution ratio D for CSB was determined by the batch method at different temperature systems (293, 309 and 321K). The distribution ratio, D, is defined as the ratio of the adsorbate concentration on the adsorbent to that in the aqueous solution and can be used as a valuable tool to study CSB mobility. The distribution ratio D is defined by the following relationship:

$K_d = q_e/C_e$ (4)

Fig. 10 shows that the distribution ratio (D) values decrease with the increase in temperatures of dye solutions. A corresponding decrease in distribution coefficient (K_d) with the increase in temperature of the sorbate solution was observed, illustrating that at higher temperatures of sorbate, lower number of sorption sites are available onto sorbent surface and the study is in agreement with earlier reported work (Xiaoming *et al*., 2016). The rapid CSB sorption has significant practical importance, as this will facilitate with the small amount of adsorbent to ensure efficiency and economy.

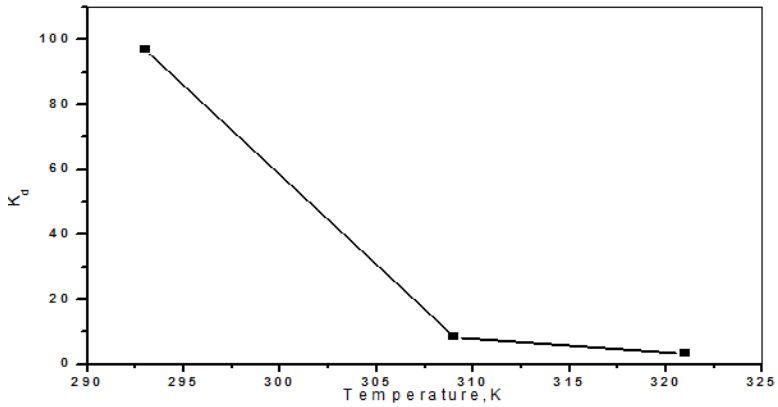

Fig. 10: The distribution coefficien of CSB

Adsorption isotherms:

The Freundlich 1906, Langmuir 1918, Temkin 1940 and Dubinin Redushkevich 1947 isotherm models were applied to the analysis of the obtained equilibrium sorption data (Figs. not shown).The Freundlich isotherm is an empirical model of a heterogeneous surface with a non-uniform distribution of heat sorption and affinities by means of multilayer adsorption.

The form of the Freundlich equation can be stated as follows:

$$\ln q_e = \log K_F + \frac{1}{n}\log C_e \quad (5)$$

where K_F ($mg^{1-1/n}/g/L^n$) and n are Freundlich constants, n indicates whether the adsorption process is favourable, and K_F is related to the adsorption capacity of the adsorbent. From the correlation coefficient value, the Freundlich equation does not agree with the experimental value (Ahmad *et al*., 2017).

The Langmuir adsorption model is based on the assumption that the maximum adsorption corresponds to a saturated monolayer of solute molecules on the adsorbent surface. Therefore, The Langmuir isotherm assumes that sorption comes from the monolayer coverage of the adsorbate over a homogenous adsorbent surface. This model supposes that sorption occurs on specific homogeneous sites within the adsorbent and that all of the sorption sites are energetically identical. The linear form of Langmuir isotherm can be written in the following form:

$$\frac{C_e}{q_e} = \frac{1}{K_L Q_{max}} + \frac{C_e}{Q_{max}} \quad (6)$$

where Q_{max} (mg/g) is the maximum amount of dye adsorbed per unit mass of adsorbent, and K_L (L/mg) is the Langmuir constant related to the rate of adsorption. C_e is the equilibrium concentration.

Temkin Isotherm:

The Temkin isotherm model suggests an equal distribution of binding energies over the number of the exchanging sites on the surface. The distribution of these energies depends on the nature of adsorbate species and the sorbent surface. The decline in the heat of adsorption is linear, but not logarithmic in nature. The linear form of Temkin isotherm can be written as:

$$q_e = B_T \ln A_T + B_T \ln C_e \quad (7)$$

where B_T = RT/b, T is the absolute temperature in Kelvin and R is the universal gas constant (8.314 J/mol/K), A_T is the equilibrium binding constant and B_T is corresponding to the heat of sorption. The results of the isotherm parameters/constants are given in Table 1. The correlation coefficient for the adsorbent (0.956) was lower than that of Freundlich and Langmuir models and showed poor linearity (Ebrahim *et al*., 2017). So, it can be said that the experimental data of CSB didn't fit to the Temkin isotherm model.

The Dubinin–Radushkevich isotherm model does not assume a homogenous surface or a constant sorption potential, as other models do. It can be noted that this isotherm model is more general than the Langmuir model. The Dubinin–Radushkevich isotherm has been written by the following equations.

$$\ln q_e = \ln X_{max} - \beta\varepsilon^2 \quad (8)$$

where β is a constant related to the adsorption energy, X_{max} is the theoretical saturation capacity, and ε is the Polanyi potential.

$$\varepsilon = RT\ln\left(1+\frac{1}{Ce}\right) \quad (9)$$

The mean free energy of adsorption (E_{DR}) defined as the free energy change when one mole of ion is transferred to the surface of the adsorbent from infinity in the solution (Somaye *et al*., 2016) was calculated by the equation, $E_{DR} = 1/(2\ \beta)^{1/2}$. The calculated D–R equation parameters and mean free energies are presented in Table 1. The magnitude of E_{DR} can be used to determine the mechanism of an adsorption process. If the E_{DR} value is in the range (8–16) kJ mol^{-1} then the adsorption process predominantly occurs through an ion-exchange mechanism, whereas for E_{DR} value <8 kJ mol^{-1} indicates a physical mechanism. In this study, the E_{DR} values are not in the range (8–16) kJ mol^{-1}) for the temperature ranges studied, suggesting that the adsorption of CSB on the adsorbent occurred through a physical mechanism (Arash *et al*., 2017).

To confirm the favorability of the CSB adsorption by the adsorbent, the separation factor (R_L) was calculated by the following equation.

$$R_L = \frac{1}{1+KLCo} \quad (10)$$

where, R_L is a dimensionless separation factor indicating the shape of the isotherm, $K_L$is the Langmuir constant and C_o is the initial adsorbate concentration. The isotherm is (i) unfavourable when $R_L > 1$, (ii) linear when $R_L = 1$, (iii) favourable when $R_L < 1$, and (iv) irreversible when $R_L = 0$. The value of R_L obtained from this study was $2.92x10^{-3}$. This R_L value are less than unity indicating that the CSB adsorption onto the adsorbent is favourable.

A non-linear regression is used to determine the best-fitting isotherm, and the applicability of the isotherm equations is compared by comparing the correlation coefficients, R^2. Table 1 shows the obtained results. The table indicates that the Langmuir equation gives the best satisfactory fitting to the adsorption isotherms of the CSB adsorption onto the adsorbent sample with higher correlation coefficients than the others (> 0.99), indicating the homogeneous nature of all the surfaces and the formation of a monolayer of CSB molecules on the surface of the adsorbent although, the Langmuir maximum adsorption capacities does not agree with the experimental value (30.23 mg/g) (Jianguo *et al*., 2016; Long *et al*., 2017; Xi *et al*., 2017).

Table 1: Adsorption isotherm models

Freundlich isotherm				Langmuir isotherm		
1/n	K_F (mg/g)	R^2	Q_{max} (mg/g)	K_L (L/mg)	R_L	R^2
0.074	36.38	0.932	29.99	4.88	$2.92x10^{-3}$	0.997
Temkin isotherm				D-R isotherm		
A_T (L/g)	B_T (J/mol)	R^2	β	X_{max} (mg/g)	E_{DR} (kJ/mol)	R^2
14.34	2.53	0.956	2.81	30.97	0.422	0.323

Kinetics study:

In order to determine and interpret the mechanisms of CSB adsorption processes and the main parameters governing sorption kinetics, empirically obtained kinetic sorption data were fitted to the pseudo-first-order (Lagergren,1898) and, pseudo-second-order (Ho, 1999) models shown in Eqs. (11) and (12), respectively (Figs. not shown). From the linear form of these three models, equations can be written as follows:

Pseudo-first-order equation:

$$\ln(q_e - q_t) = \ln q_{e,1} - k_1 t \quad (11)$$

where q_e and q_t are the sorption capacity (mg/g) at equilibrium and time t, respectively, k_1 is the rate constant (L min^{-1}) of pseudo-first-order kinetic model. From the correlation coefficient value, the pseudo-first-order equation does not agree with the experimental value (Roohan and Yasaman, 2017).

Pseudo-second-order equation:

$$\frac{t}{q_t} = \frac{1}{k_2 q_{e,2}^2} + \frac{t}{q_{e,2}} \quad (12)$$

The initial adsorption rate (h) can be determined from k_2 and q_e values using

$$h = k_2 qe^2 \quad (13)$$

where k_1 and k_2 are the adsorption rate constants of first and second order kinetic models, in min^{-1} and L (mg $min)^{-1}$, respectively; q_e and q_t in mg g^{-1}, are equilibrium adsorption uptake (at time $t = \infty$) and adsorption uptake (at time t), respectively.

The calculated kinetic parameters for adsorption of CSB dye ions on the adsorbent, at an initial concentration of 70 mg/l is presented in Table 2, where it can be seen that the pseudo-second-order equation appears to be the best fitting model than those for the other two equations (the correlation coefficient is extremely high for the pseudo-second-order equation of the adsorbent; $R^2 > 0.9999$). From the Table 2, we can observe the change of the initial adsorption rate h (mmol/(g min)) values of CSB onto the adsorbent, when the temperature increased. Similar results have been reported about the adsorption of dyes onto the different adsorbents in the literatures (Somayeh *et al*., 2017; Agnès *et al*., 2017).

Table 2: Adsorption kinetic models

	The pseudo-first-order				The pseudo-second-order			
T(K)	$q_{e,exp}$ (mg/g)	$q_{e,1,cal}$ (mg/g)	K_1 (min^{-1})	R^2	$q_{e,2,cal}$ (mg/g)	K_2 (g/mg min)	h (mg/g min)	R^2
293	34.85	1.11	0.0183	0.95632	35.24	0.0075	9.26	0.99997
309	33.20	1.16	0.01579	0.93521	33.46	0.0061	6.8	0.99996
321	30.41	1.11	0.02298	0.94737	30.76	0.0100	9.49	0.99998

This consistency of the experimental data with the pseudo-second-order kinetic model indicates that the rate limiting step for the adsorption of CSB ion on the adsorbent mixed oxides is chemical adsorption, which involves valence forces through sharing or exchange of electrons between adsorbent and adsorbate, with no involvement of a mass transfer in solution . As a result, the adsorption of the CSB dye onto the adsorbent can be considered to involve two processes with the initial adsorption rate on the adsorbent. This adsorption rate is related to the content and type of active adsorption site on the adsorbent matrix.

Adsorption mechanisms:

The overall solute adsorption onto the solid surface may be controlled by one or more steps, e.g., boundary layer (film) or external diffusion, pore diffusion, surface diffusion and adsorption onto the pore surface or in combination of several steps. An empirically found functional relationship, i.e. the Weber–Morris plot, common to the most adsorption processes, is that the uptake varies almost proportionally with $t^{0.5}$, rather than with contact time (Weber, 1963). Generally, intraparticle diffusion mechanism is one of the most limiting factors which controlled adsorption kinetics. The linearized intraparticle diffusion model is given as Eq. (14):

$$qt = K_i t^{0.5} + C \quad (14)$$

where C (mg g^{-1}) is the intercept and K_i is the intraparticle diffusion rate constant (mg g^{-1} $min^{-0.5}$), which can be calculated from the slop of the linear plots of q_t versus $t^{0.5}$ (Fig. 11).

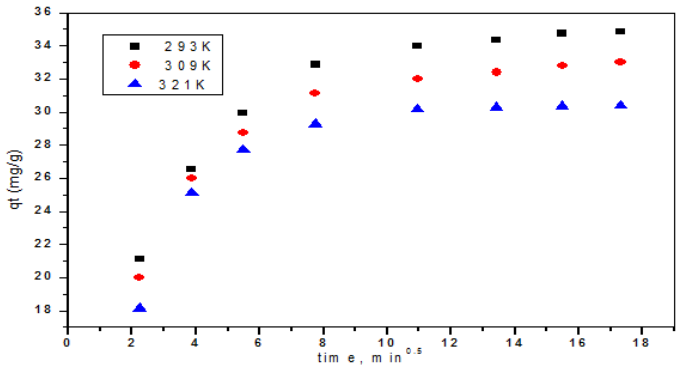

Fig. 11: Intraparticle diffusion plots of CSB at different tem peratures

Adsorption kinetics are generally controlled by different mechanism, of which the most limiting are diffusion mechanisms, including an initial curved portion, attributed to rapid external diffusion or boundary layer diffusion and surface adsorption, and a linear portion, a gradual adsorption stage due to intraparticle diffusion, followed by a plateau to equilibrium where the intraparticle diffusion starts to decrease due to the low concentration in solution phase as well as fewer available adsorption sites. If the regression of q_t versus $t^{0.5}$ is linear and passes through the origin, then intraparticle diffusion is the sole rate-limiting step. However, by the plots of q_t versus $t^{0.5}$ of different Chicago Sky Blue solution temperatures, multi linearities are observed in Fig. 11, indicating that two steps took place during Chicago Sky Blue adsorption onto the adsorbent. Two following steps are thought to be involved during the adsorption of the dye on the adsorbent. Firstly, Chicago Sky Blue in aqueous solution was transported onto the surface of the adsorbent (film diffusion). Subsequently, the Chicago

Sky Blue dye was transported and adsorbed on the interior surface of the adsorbent (Mohammed *et al*., 2015; Xiang *et al*., 2017). In fact, SEM and BET analyses have proven than the uneven surface of the adsorbent enhanced adsorption active sites and provided an advantageous condition for attracting more target pollutants around adsorption active sites and correspondingly improved the rate of adsorption and adsorption capacities.

Effect of temperature and thermodynamic studies:

The fraction of CSB dye removal as a function of temperature (Fig. 12) shows that adsorption removal percentage decreases from 99.15 to 86.51% with a rise in the temperature from 293 to 321K. This further supports the surface heterogeneity of oxide surfaces. The observation shows that the interaction between adsorbate and adsorbent is exothermic in nature. Even the change in the temperature does not influence the equilibrium time (300 min) and the removal curve is smooth and continuous (Shuheng *et al*., 2016; Xiang *et al*., 2017).

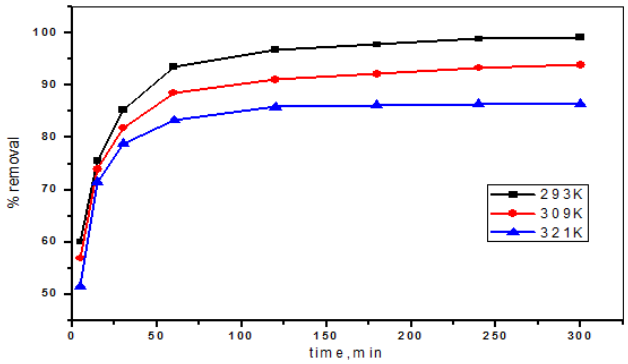

Fig. 12: Effect of temperature on the % removal of CSB

The temperature dependence of adsorption process is associated with changes in several thermodynamic parameters such as the free energy (ΔG), the enthalpy change (ΔH) and the entropy change (ΔS)

Thermodynamic parameters:

Thermodynamic parameters, enthalpy ΔH (kJ mol^{-1}), entropy ΔS (J mol^{-1} K^{-1}) and standard free energy of activation ΔG (kJ mol^{-1}) were investigated in the range of 293–321 K under the optimized conditions chosen by applying the equations (15,16):

$$\ln K_d = \frac{\Delta S}{R} - \frac{\Delta H}{RT} \quad (15)$$

$$\Delta G = -RT\ln K_d \quad (16)$$

Where 'R' is a gas constant, 'T' is the temperature in Kelvin.

The plots of log K_d versus 1/T (K^{-1}) are linear throughout the investigation (Fig. not shown) and the values of ΔH and ΔS are computed from the respective slopes and intercepts of the plots. The calculated thermodynamic parameters are presented in Table 3.

The negative values of (ΔG^o) show that the CSB dye adsorption by the adsorbent is spontaneous in nature (Table 3). Furthermore the decrease in ΔG^o values with an increase in temperature indicates that the adsorption of CSB dye is favourable at low temperature. The negative value of enthalpy change (ΔH^o) obtained for the adsorption of CSB (Table 3) is indicative of the exothermic nature of the adsorption process (Xi-Ping *et al*., 2017; Zongjun *et al*., 2017). The negative entropy change (ΔS^o) for this reaction also indicates a decrease in the number of species at the solid–liquid interface and, hence a decrease in randomness in the (solid - liquid) interface with an increase in temperature (Fang *et al*., 2017).

Table 3: Thermodynamic parameters.

Temp.K	ΔG (KJ/mol)	ΔS (J/molK)	ΔH (KJ/mol)	R^2	Ea (KJ/mol)	S^*	R^2
293	- 11.13	- 293	- 967	0.945	78.22	$1.21x10^{-12}$	0.964
309	- 5.24						
321	- 3.12						

In order to further support the assertion that the adsorption is the predominant mechanism, the values of the activation energy (E_a) and sticking probability (S*) were estimated from the experimental data. They were calculated using a modified Arrhenius type equation (Singh *et al*., 2013) related to surface coverage as expressed in equations (17,18):

$$\theta = 1 - \frac{C_e}{C_0} \quad (17)$$

$$S^* = (1 - \theta) \exp\left(-\frac{E_a}{RT}\right) \quad (18)$$

The apparent activation energy (E_a) and the sticking probability (S*) are estimated from the plot (Fig. not shown). The sticking probability, S*, is a function of the adsorbate/adsorbent system under consideration and is dependent on the temperature of the system. The parameter S* indicates the measure of the potential of an adsorbate to remain on the adsorbent indefinitely. It can be expressed as in Table (3).The effect of temperature on the sticking probability was evaluated throughout the temperature range from 293 to 323 K by calculating the surface coverage at the various temperatures. Table (3) also indicated that the values of $S^* \leq 1$. Hence the sticking probability of the CSB dye onto the adsorbent system is very high.

The calculated Ea for the adsorption of CSB on the adsorbent sample is 78.22kJ/mol, indicating chemical adsorption occurred in the process of CSB dye adsorbed on the sample. The positive value of the apparent activation energy E_a also indicated that the lower solution temperature favours the adsorption process and also the adsorption process is exothermic in nature (Xin *et al*., 2015).

Conclusion:

The adsorbent was used as adsorbent for the removal of typical azo dye (Chicago Sky Blue) from aqueous solution. The initial concentration, contact time, temperature, adsorbent dosage and pH on the adsorption played a significant role in the dye adsorption capacity of the adsorbent. The maximum adsorption capability of Chicago Sky Blue on the adsorbent reached 34.85 mg g^{-1} at pH=7.8. The pseudo-second-order model fitted to experimental data well. Isotherm modelling revealed that the Langmuir equation could better describe the adsorption of CSB on the adsorbent as compared to Freundlich model. Negative values of free energy change, $\Delta G°$, indicated that adsorption of CSB by the adsorbent was spontaneous. Changes in enthalpy $\Delta H°$ and entropy $\Delta S°$ also indicated negative values, and therefore, the adsorption mechanism is found to be exothermic. The generated data can be used as baseline data for designing treatment plants for the treatment of dye containing effluents. For the removal of azo dyes from wastewater with the adsorption method, it is a promising route to graft functional polymer on the solid supports with high performance.

References

Ahmad, R.B., M. Ghaedi, A. Asfaram, A.A. Bazrafshan, R. Jannesar, 2017. Ultrasonics Sonochemistry, 34: 294-304.

Agnès, B., L. Obeid, R. Mbolantenaina, M. Welschbillig, D. Talbot, 2017. Journal of Magnetism and Magnetic Materials, 421: 59-64.

Arash, A., M. Ghaedi, S. Hajati, A. Goudarzi, E.A. Dil, 2017. Ultrasonics Sonochemistry, 34: 1-12.

Biswas, K., K. Gupta, U.C. Ghosh, 2009. Chemical. Engineering. Journal., 149: 196-206.

Boran, W., L. Su, X. Dai, X. Chai, 2017. Chemical Engineering Journal, 307: 418-426.

Bouazizi, A., M. Breida, A. Karim, B. Achiou, M. Ouammou, J.I. Calvo, A. Aaddane, K. Khiat, S.A. Younssi, 2017. Ceramics International, 43: 1479-1487.

Carmen, S.D.R., S.A.C. Carabineiro, F.J. Maldonado-Hódar, L.M. Madeira, 2017. Catalysis Today, 280: 165-175.
Chunsheng, L., X. Zhu, B. Zhu, C. Jiang, Y. Le, J. Yu, 2017. Journal of Hazardous Materials, 321: 801-811.
Dordio, A.V., S. Miranda, J.P. P. Ramalho, A.J. P. Carvalho, 2017. Journal of Hazardous Materials, 323, Part A, 575-583.
Dubinin, M.M., L.V. Radushkevich, 1947. Chem. Zentr, 1: 875-889.
Ebrahim, A.D., M. Ghaedi, A. Asfaram, 2017. Ultrasonics Sonochemistry, 34: 792-802.
Edson, L.F., S. Battiston, J.M. Simões, M.M. Bassaco, L.S.F. Pereira, É.M.M. Flores, E.I. Müller, 2012. Microporous and Mesoporous Materials, 163: 29-33.
Erol, A., M. Bulut, A.Ü. Metin, H. Çiftçi, 2017. Spectrochimica Acta Part A: Molecular and Biomolecular Spectroscopy, 171: 132-138.
Fan, Y., Q. Jiang, M. Zhu, L.Zhao, Y. Zhang, 2017. Science of The Total Environment, 577: 54-60.
Fang, Z., L. Li, J. Xing, 2017. Journal of Hazardous Materials, 321: 103-110.
Farhadi, S., S. Panahandehjoo, 2010. Applied. Catalysis. A: Gen., 382: 293-302.
Freundlich, H.M.F., 1906. Über die adsorption in lösungen. Z. Phys. Chem. (Leipzig) 57A, 385-470.
Fu, Y., T. Viraraghavan, 2002. Adv. Environmental. Research, 7: 239-247.
Hemant, S., G. Chauhan, A.K. Jain, S.K. Sharma, 2017. Journal of Environmental Chemical Engineering, 5: 122-135.
Ho, Y.S., G. McKay, 1999. Process. Biochem., 34: 451-465.
Jianguo, Z., Y.Wang, J. Wang, W. Qiao, D. Long, L. Ling, 2016. Journal of Colloid and Interface Science 462: 200-207.
Jun, H.,1.H. Xiea, H. Yea, T. Xiea, Y. Lina, J. Gonga, C. Jianga, Y. Wua, S. Liua, Y. Cuib, J. Mao, L. Meic, 2016. Carbohydrate Polymers 138: 301-308.
Kanna, M., W. Sumpun, 2008. Materials, Chemical and Physics., 110: 166-175.
Khadijeh, A., H. Tayebi, 2017. Spectrochimica Acta Part A: Molecular and Biomolecular Spectroscopy, 171: 439-448.
Lagergren, S.,1898. Handlingar, 24(4): 1-39.
Langmuir, I., 1918. J. American of Chemical. Society, 40: 1361-1403.
Lin, W., H. Gu, J. He, T. Zhao, X. Zhang, C. Xiao, H. Liu, X. Zhang, Y. Li, 2017. Journal of Alloys and Compounds, 695: 599-606.
Long, C., Q. Yanhui Li, Z. Du, Wang, Y. Xia, E. Yedinak, J. Lou, L. Ci, 2017. Carbohydrate Polymers, 155: 345-353.
Lu, Y.g., F. Wang, A. Hakki, D.E. Macphee, P. Liu, S. Hu, 2017. Applied Surface Science, 392: 687-696.
Mane, V.S., P.V.V. Babu, 2013. J. Taiwan Inst. Chem. Eng., 44: 81-88.
Mayur, B.K., T.R. Waghmode, S.M. Patil, B. Jeon, S.P. Govindwar, 2017. Chemical Engineering Journal, 307: 1026-1036.
Mei-Yu, G., D. Xu, Y. Song, Y. Guo, 2013. Sensors and Actuators B: Chemical., 188: 1148-1154.
Mena, E., A. Rey, E.M. Rodríguez, F.J. Beltrán, 2017. Catalysis Today, 280(1): 74-79.
Mohammed, K., M. Trari, R. Maachi, N. Nasrallah, B. Bellal, A.Amrane, 2015. Journal of Environmental Chemical Engineering, 3: 548-559.
Muhammad, S., H. Tahir, J. Khan, U. Hameed, A. Saud, 2017. Ultrasonics Sonochemistry, 34: 600-608.
Nishimura, H., G. Nelson, W. Rosenblum, 1989. Microcirc Endothelium Lymphatics, 5(6): 435-40.
Petrick, A.S., R. Souza, J. Soler, T.F.C.V. Silva, S.M.A.G.U. Souza, Rui A.R. Boaventura, V.J.P. Vilar, 2017. Separation and Purification Technology, 172: 450-462.
Pigorsch, E., A. Elhaddaoui, S. Turrel, 2013. Spectrochim. Acta, Part A, 50: 2145-2152.
Roohan, R., N. Yasaman, 2017. Journal of Magnetism and Magnetic Materials, 422: 128-140.
Shuheng, Y., J. Zhang, D. Shen, R. Xiao, S.Gu, M. Zhao, J. Liang, 2016. Journal of Colloid and Interface Science, 463: 118-127.
Sílvia, C.R.S., R.A.R. Boaventura, 2016. Journal of Environmental Chemical Engineering, 4: 1473-1483.
Singh, B., S.K. Das, 2013. Colloids and Surface. B: Biointer., 107: 97-106.

Sneha, C., H. Uppal, M. Yadav, N. Bahadur, N. Singh, 2017. Ecotoxicology and Environmental Safety, 135: 68-74.

Somayeh, D., M. Ghaedi, A. Asfaram, F. Zare, S. Wang, 2017. Ultrasonics Sonochemistry, 34: 343-353.

Somaye, M., R. Sohrabi, H. Javadian, M. Ghasemi, Inderjeet Tyagi, Shilpi Agarwal, Vinod Kumar Gupta, 2016. Journal of Molecular Liquids, 215: 144-153.

Temkin, I.M., V. Pyzhev, 1940. Acta Physiochem. SSR 12: 217-222.

Thines, K.R., E.C. Abdullah, N.M. Mubarak, M. Ruthiraan, 2017. Renewable and Sustainable Energy Reviews, 67: 257-276.

Weber, J.W.J., J.C. Morris, 1963. Journal Sanitary Engeering Division Proceedings.American Society of Civil Engineers, 89: 31-59.

Wei, Z., W. Zhang, Z. Chen, 2017. Applied Surface Science, 392: 153-161.

Xi-Ping, L., S. Fu, Y. Du, J. Guo, Bing Li, 2017. Microporous and Mesoporous Materials, 237: 268-274.

Xi, Z., J. Wang, S. Chen, Z. Bao, H. Xing, Z. Zhang, B. Su, Q. Yang, Y. Yang, Q. Ren, 2017. Separation and Purification Technology, 172: 43-50.

Xin[a], S., R. Wang, W. Zhao, S. Sun, C. Zhao, 2017. 2[nd]- Journal of Colloid and Interface Science, 485: 39-50.

Xin[b], H., B. Gao, Y. Sun, Q. Yue, Y. Wang, Q. Li, X. Xu, 2017. Separation and Purification Technology, 173: 209-217.

Xiang, H., H. Zhang, Z. Sun, 2017. Applied Surface Science, 392: 332-341.

Xiaoming, H., M. Pan, 2016. Journal of Molecular Liquids, 215: 410-416.

Xiaoyun, S., S. Zheng, J. Zhang, W. Li, Q. Chen, B. Cao, 2012. Materials Research Bulletin, 47: 4305-4310.

Ying-Lung, H., Y. Lo, C. Cheng, W. Yu, D. Nagarajan, C. Liu, Y.Li, J.Chang, 2017. Biochemical Engineering Journal, 117(A): 48-56.

Yue, C., X. Liu, T. Chung, M. Weber, C. Staudt, C. Maletzko, 2016. Water Research, 91: 104-114.

Yunchuan, Q., M. Yang, W. Xu, S. He, Y.Men, 2017. Journal of Colloid and Interface Science, 486: 84-96.

Zhenzhen, H., G. Chen, G. Zeng, Z. Guo, K. He, L. Hu, J. Wu, L. Zhang, Y. Zhu, Zhongxian Song, 2017. Journal of Hazardous Materials, 321: 37-46.

Zhijie, L., Z. Zhao, T. Sun, W. Shi, F. Cui, 2017. Journal of Colloid and Interface Science, 485: 192-200.

Zongjun, D., Y. Zhang, Z. Li, H. Chen, Y. Wang, G. Wang, P. Zou, H. Chen, Y. Zhang, 2017. Applied Surface Science, 392: 312-320.